Composites: Part B 45 (2013) 148–158

Contents lists available at SciVerse ScienceDirect

Composites: Part B

journal homepage: www.elsevier.com/locate/compositesb

An analysis of the stress–strain state of a timber–concrete *T* cross section

Darius Zabulionis [a,*], Olga Kizinievič [b], Luciano Feo [c]

[a] Vilnius Gediminas Technical University, Institute of Mechanics, Saulėtekio al 11, Lithuania
[b] Vilnius Gediminas Technical University, Department of Building Materials, Saulėtekio al 11, Lithuania
[c] Department of Civil Engineering, University of Salerno, 84084 Fisciano (SA), Italy

ARTICLE INFO

Article history:
Received 10 January 2012
Received in revised form 22 September 2012
Accepted 25 September 2012
Available online 8 October 2012

Keywords:
A. Layered structures
B. Strength
C. Laminate mechanics
C. Analytical modelling
Timber–concrete composites

ABSTRACT

The present paper analyzes a stress–strain state of a composite timber–concrete *T* cross section under a short-term pure bending. The behaviour of a bending moment in respect of a curvature of the cross section was investigated as well. It is assumed that the plane section hypothesis is valid and layers do not slip with respect to each other. The parabolic stress–strain diagram with a descending branch, according to MC90, was applied to the compression concrete while a linear elastic relationship was applied to the timber. The stress–strain state of the cross section was investigated from the beginning of the loading up to the stage exceeding ultimate limit state. The analysis was conducted by applying control of the curvature of the considered cross section. The influence of the tension fibre-reinforced polymer (FRP) and compression steel reinforcements on the stress–strain state of the cross section was also considered. The obtained analytical equations of the layered members were solved numerically. It was found out that the bearing capacity of the cross section is restricted mainly due to low strength of the timber and the tension reinforcement is more effective than the compression reinforcement.

1. Introduction

Timber concrete composite (TCC) structures have been studied intensively in recent years. Experimental, analytical and numerical investigations include short-term and long-term behaviour of the TCC structures with various connectors under thermal and moisture actions, taking into account shrinkage of the concrete, nonlinear behaviour of the materials of the layers as well as a nonlinear slip between interfaces of the layers. The recent literature review on TCC was made in [1]. The solid TCC floor system whose interfaces were with notches cut and with anchors, under a short-term loading, experimentally and numerically with a finite-element method was investigated by Gutkowski et al. [2,3]. Adhesive bonded double *T* cross section timber-ultra-high-concrete composite beams with a glued joint under cyclic and static loads were tested by Schäfers [4]. Thin-webbed TCC beams, with a wall made out of oriented strand board, under a short-term loading were tested by Gurkšnys [5]. TCC beams with various connectors under short-term and long-term loadings were tested by Ceccoti et al. [6], Lukaszewska et al. [7], Negrão et al. [8], Fragiacomo et al. [9,10], Mueller et al. [11], Jorge et al. [12].

Along with experimental investigations, the analytical methodologies have also been developed to calculate the TCC beams and plates. Perhaps, the earliest exact methodology of an elastic multilayered beam with an interlayer slip of each interface was developed by Rzhanicyn in 1948 [13]. The effect of the uplift of the interlayer and the nonlinear behaviour of the interfaces were also considered [14]. The methodology how to calculate build-up bars according to the plastic limit state was also developed in [14]. Rzhanicyn also developed a theory for the build-up plates [14]. Some methodologies for TCC taking into account the slip between interfaces of the layers are given in [15–19]. Theoretical analysis of three layered timber–concrete beam and comparison with experiment is given in [20].

When the plane section hypothesis is valid, then there are other methodologies suitable for TCC structures. The majority of these methodologies were developed for the reinforced concrete structures, for example [21,22].

The finite element method is also used to analyze the behaviour of the TCC beams subject to short-term and long-term loading, taking into account the shrinkage of concrete, the moisture and thermal expansions of concrete whether timber [2,7,10]. The creep of the joint is also taken into account. The properties of the concrete were taken according to MC90 [23].

It is evident that the behaviour of the cross section depends on the stiffness of the connections of the layers. In general, bending of TCC members shall be considered taking into account an interlayer slip. However, the behaviour of the cross sections of the beam depends not only on the stiffness of the interface but also on the length of the beam, its support and loading conditions. Stiffness

* Corresponding author.
E-mail addresses: darius.zabulionis@vgtu.lt (D. Zabulionis), olga.kizinievic@vgtu.lt (O. Kizinievič), l.feo@unisa.it (L. Feo).

1359-8368/$ - see front matter © 2012 Elsevier Ltd. All rights reserved.
http://dx.doi.org/10.1016/j.compositesb.2012.09.082

Nomenclature

Latin symbols

$\|\cdot\|$	absolute value
A and A_i	areas of the whole cross section and ith layer respectively
A_{FRP}	cross section of FRP
A_s	cross section of reinforcement
a_s	distance between the top of the cross section and the centroid of reinforcement
b_i	width of ith layer
D	discriminant
E_{ci}	initial tangent modulus of concrete
E_{cm}	secant modulus of elasticity of concrete
E_{FRP}	modulus of elasticity of FRP
E_s	modulus of elasticity of steel
E_w	modulus of elasticity of timber
f_{cm}	mean cylinder strength of concrete
f_w	strength of timber
f_y	yield point of steel
$f_{\sigma,c}(\varepsilon)$, $f_{\sigma,c,I}(\varepsilon)$ and $f_{\sigma,c,II}(\varepsilon)$	stress–strain relationships of concrete
$f_{\sigma,FRP}(\varepsilon)$ and $f_{\sigma,w}(\varepsilon)$	stress–strain relationships for FRP and timber respectively
$f_{\sigma,i}(\varepsilon)$	stress–strain relationship for ith layer
G	shear modulus
h and h_i	are heights of the whole cross section and ith layer respectively
h_{jnt}	thickness of joint
$J(\cdot)$	stress–slip relationship of a joint
M	bending moment
M_k	characteristic bending moment of a cross section
M_{max}	local maximum of the bending moment
$M_{\varepsilon cu1}$	bending moment when the strain of concrete equals to ε_{cu1}
$M_{\varepsilon w,lim}$	bending moment when strain of timber equals to its limit value $\varepsilon_{w,lim}$
N	axial force
n	number of the layers
s	interlayer slip
S_i	first order moment of ith area
y and z	coordinates

Greek symbols

$\varepsilon_{c,lim}$	strain of the compressive concrete at $0.5\,f_{cm}$
ε_{cu1}	limit strain of the compressive concrete for bending members according to EC2
γ	shear angle
δ_i	distance between the neutral axis and top edge of the ith layer
δ_s	distance between the neutral axis and the centroid of the steel reinforcement
ε	strain
$\varepsilon^*_{max,c}$	maximal strain of concrete corresponding to a local maximum of the bending moment
$\varepsilon^*_{min,w}$	minimal strain of timber corresponding to a local maximum of the bending moment
ε_{c1}	compressive strain of concrete corresponding to its maximum stress
ε_{max} and ε_{min}	maximal and minimal strains at the top and bottom of the cross section respectively
$\varepsilon_{max,c}$	maximal strain of concrete
$\varepsilon_{min,w}$	minimal strain of timber
$\varepsilon_{w,lim}$	limit strain of timber
ζ	position of the neutral axis
ζ_{el}	position of the neutral axis of the elastic cross section
η and η_0	stiffness and initial stiffness of a joint respectively
κ	curvature
κ^*	curvature corresponding to the maximal bending moment
ξ	coefficient
ρ_s and ρ_{FRP}	reinforcement ratios for steel and FRP reinforcements
σ_c	stresses of concrete
$\sigma_i(\cdot)$	function describing the distribution of the normal stresses through the depth of the cross section
σ_w	stresses of timber
τ	tangential stresses
$\varphi_{i,1}(z)$ and $\varphi_{i,2}(z)$	functions describing the region of the cross section
$\Psi(z)$	function describing distribution of the strain through the depth of the cross section
Ω_i	domain of the ith layer

of the interface depends on the type of connectors. Perhaps, the stiffest connectors are glued joints, whose stiffness depends on the thickness of the joint [1,8,24]. When the thickness of the joint tends to zero, then its initial stiffness or its initial slip modulus tends to infinity. Here, the initial stiffness of the joint is treated as the value of the slip derivative of the stress–slip relationship as the slip equals zero. That is, the initial stiffness of the joint $\eta_0 = [dJ(s)/ds]_{s=0}$, where s and $J(s)$ are the interlayer slip and stress–slip relationship of a joint, respectively. Let us illustrate this assertion by employing the linear elastic stress–slip relationship for a joint, i.e. $\tau = \eta s$, where η and s are stiffness of the joint and slip, respectively. According to the Hooke law $\tau = \gamma G$, where γ and G are shear angle of the joint and shear modulus, respectively. If assumption of the small displacement is valid, then $\gamma = \tan(\gamma) = s/h_{jnt}$, where h_{jnt} is thickness of the joint. By equating $\tau = \eta s$ and $\tau = \gamma G = (G\,s/h_{jnt})$ we get $\eta = G/h_{jnt}$. Therefore, $\eta \to \infty$ as $h_{jn} \to 0$. Given explanation is also valid for nonlinear joint whose stress–slip relationship is linear or very close to the linear relationship at small slip, i.e. as $s \to 0$. The plane sections' hypothesis may be applied practically to every cross section of such bending members. This assumption was made in the research [8]. Notches cut in the timber and continuous connectors glued to the timber are also very stiff connectors [1,8,24]. When a joint is made with screws, nail plates or dowels, the plane section hypothesis cannot be applied to each cross section of the beam.

The stiffness of the joint can be characterized by the slip modulus. However, the characterization of the stiffness of the nonlinear joint by the slip modulus is not comprehensive. Therefore, several criteria were suggested how to evaluate the efficiency of the composite beams and their joints [2,19]. The most popular evaluation is as follows $EFF = (w_{NC} - w_{PC})/(w_{NC} - w_{FC}) \cdot 100\%$, where w_{NC}, w_{PC} and w_{FC} denote the deflections of the midspan of the composite beam with absolutely slender, partially stiff, and absolutely stiff connections, respectively. Instead of the deflections the areas and volumes between the positions of the cross section before loading and after it were also applied to *EFF* [2]. The mentioned efficiency involves not only the stiffness of the joint, but also the length of the beam. Since w_{PC} tends to w_{FC} as the length of the beam tends to infinity, then it is evident that the *EFF* increases up to 100% with increasing the length of the beam. Therefore, it is possible to evaluate whether the plane section hypothesis is valid for certain cross sections if *EFF* is big enough. As reported in [7], the efficiency of the TCC beams can reach 98%. Thus, if both the length of the beam and the stiffness of the joint are big enough, there are cross sections in the beam for which the plane section hypothesis is valid. In the case of a simple supported symmetrically loaded beam, these cross

sections are in the middle of the beam with respect to its length. Such cross sections can be calculated neglecting the interlayer slip.

As is known, the bilinear stress–strain diagram shall be applied for bending members according to EC2 [25]. In [8], this diagram was applied in order to investigate the influence of the nonlinearity of the concrete behaviour in comparison with the linear elastic constitutive law. On the other hand, according to EC2 [25], a parabolic stress–strain diagram may be also adopted for the analysis of the cross-section. This diagram and the bilinear stress–strain diagram are restricted up to so-called ultimate compressive strain. However, in some cases, it is important to determine the pure carrying capacity of the cross section, when accidental actions affect structures. In this case, some restrictions of the design codes can be violated. Therefore, according to MC90 [23], a full parabolic stress–strain diagram is adopted in the present investigation.

2. Governing equations

Let us consider the cross section of a prismatic layered member with the following assumptions:

1. the contact between layers is perfect, i.e. no slip occurs between the interfaces of layers;
2. the prismatic element is in pure plane bending conditions; that is, the stress–strain state is uniaxial;
3. the plane section hypothesis is valid;
4. the prismatic element is bent around the principical axis of the cross section (Fig. 1);
5. the shape and size of the cross section remains unchanged during the bending.

The second assumption was made in order to restrict the area of our investigations. In pure bending condition the uniaxial stress state occurs in the cross-section. Therefore, only normal stresses should be calculated in order to examine the stress–strain state and load-carrying capacity of the cross section. Otherwise, in case of shear forces and bending moment the tangential stresses must be calculated beside the normal stresses as well. It complicates analysis, because it is more difficult to calculate tangential stresses than normal stresses. O the other hand, in plane stress state more sophisticated failure criteria should be applied for concrete as well.

Under the aforementioned assumptions, the following conditions of static equilibrium can be written for the whole cross section of the layered element:

$$N = \sum_{i=1}^{n} \iint_{A_i} \sigma_i(z)\,dz\,dy = 0 \tag{1}$$

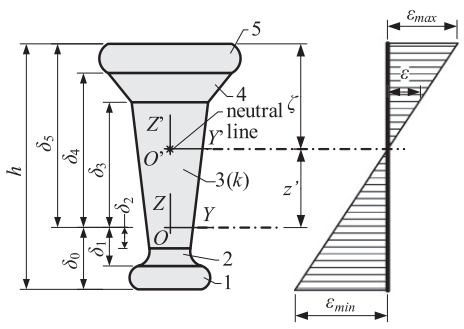

Fig. 1. Cross-section of a prismatic layered member and distribution of strain through its depth.

$$M = \sum_{i=1}^{n} \iint_{A_i} (z - z')\sigma_i(z)\,dz\,dy \tag{2}$$

where $\sigma_i(\cdot)$ is a function describing the distribution of the normal stresses through the depth of the cross section of the ith layer, axial force N and bending moment M are resultants of the internal forces of the cross section, z' is the coordinate of the neutral axis of the cross section in an arbitrary frame of reference YOZ, A_i is the area of the cross section of the ith layer, n is the number of the layers (Fig. 1). The total area of the cross section is as follows $A = \sum_{i=1}^{n} A_i$. It is also assumed that the compressive stresses and strains are negative while the tensile stresses and strains are positive.

It should be noted that beside bending load an axial force may affect a TCC structure. In general, an analysis of such structures is more complicated due to buckling. Axial forces affect the position of the neutral axis and an arrangement of the stresses through the depth of the cross section. However, if the resultants of the external forces are known, taking into account second order effects caused by structural deformations, then an analysis of the stress–strain state and ultimate limit state of the cross-section can be conducted by Eqs. (1) and (2) as well. In this case Eq. (2) remains unchanged, however, the resultant of the axial force N, in Eq. (1), does not equal zero.

The validity of the plane section hypothesis means that the strain state through the depth of the cross section of the layered element can be completely defined by two parameters: the position of the neutral axis ζ and the strain ε at a certain point of the cross section or by the position of the neutral axis ζ and the curvature κ of the deformed axis. Let the distribution of the strains through the depth of the cross section be described by a linear function $\Psi(z)$ which may be defined as follows:

$$\varepsilon(z) = \Psi(z) = \frac{1}{\beta}(z - z') \tag{3}$$

where β is as follows: $\beta = \zeta/\varepsilon_{max}$, $\beta = (\zeta - h)/\varepsilon_{min}$, or $\beta = 1/\kappa$. Where ε_{min} and ε_{max} are minimal and maximal strain at the edges of the cross section, ζ is the distance between the neutral axis and the outer top surface of the cross section (Fig. 1), κ is the curvature and h is the depth of the whole cross section.

Let the stress–strain relationship of the ith layer be $f_{\sigma,i}(\varepsilon)$. Then, taking into account Eq. (3), the dependence of the stresses through the depth of the cross section of the ith layer is $\sigma_i(z) = f_{\sigma,i}(\Psi(z))$. The integrals in (1) and (2) can be rewritten as repeated ones. If we assume that the normal stresses σ depend only on the coordinate z, then the integrals (1) and (2) can be integrated one time with respect to the y:

$$N = \sum_{i=1}^{n} \int_{\delta_{i-1}}^{\delta_i} f_{\sigma,i}(\Psi(z))(\varphi_{i,2}(z) - \varphi_{i,1}(z))\,dz = 0 \tag{4}$$

$$M = \sum_{i=1}^{n} \int_{\delta_{i-1}}^{\delta_i} (z - z') f_{\sigma,i}(\Psi(z))(\varphi_{i,2}(z) - \varphi_{i,1}(z))\,dz \tag{5}$$

where $\varphi_{i,2}(z)$ and $\varphi_{i,1}(z)$ are functions describing the region of the cross section of the ith layer in the frame of reference YOZ, δ_i is the coordinate of the ith layer edge in the YOZ (Fig. 1) given by,

$$\delta_i = (\zeta + z') - h + \sum_{j=1}^{i} h_j \tag{6}$$

where h_i is the thickness of the ith layer and h is the thickness of the whole cross section i.e. $h = \sum_{i=1}^{n} h_i$. In Eq. (7) it is assumed that $\sum_{j=1}^{0} h_j = 0$.

If the cross sections of all layers are rectangular, then $\varphi_{i,1}(z) = -1/2\ b_i$ and $\varphi_{i,2}(z) = 1/2\ b_i$, where b_i is the width of the

ith layer. Then Eqs. (4) and (5) can be expressed as follows:

$$N = \sum_{i=1}^{n} b_i \int_{\delta_{i-1}}^{\delta_i} f_{\sigma,i}(\Psi(z))dz = 0$$
$$M = \sum_{i=1}^{n} b_i \int_{\delta_{i-1}}^{\delta_i} (z - z') f_{\sigma,i}(\Psi(z))dz \tag{7}$$

Let us substitute the strain ε for coordinate z in integral (7), where ε is given in (3). Eq. (3) yields:

$$z = \varepsilon\beta + z' \tag{8}$$

Then substitution Eqs. (8) into (7) yields:

$$N = \beta \sum_{i=1}^{n} b_i \int_{\varepsilon_{i-1}}^{\varepsilon_i} f_{\sigma,i}(\varepsilon)d\varepsilon = 0$$
$$M = \beta^2 \sum_{i=1}^{n} b_i \int_{\varepsilon_{i-1}}^{\varepsilon_i} \varepsilon f_{\sigma,i}(\varepsilon)d\varepsilon \tag{9}$$

where the new integration limits ε_{i-1} and ε_i are strain at the bottom and top of the ith layer, respectively:

$$\varepsilon_i = \frac{1}{\beta}(\delta_i - z') = \frac{1}{\beta}\left(\zeta - h + \sum_{j=1}^{i} h_j\right), \quad i = 0, 1, \ldots, n \tag{10}$$

where δ_i is given in (6) and $\sum_{j=1}^{0} h_j = 0$. From (10) we get: when $i = 0$ then $\varepsilon_0 = \varepsilon_{min}$ and when $i = n$ then $\varepsilon_n = \varepsilon_{max}$.

We should emphasize that Eqs. (9) and (10) are written for the frame of reference $Y'O'Z'$ (Fig. 1). Eq. (9) may be more convenient than Eq. (7) because the stress–strain relationships are integrand in (9) and integration can be performed directly without any transformation of the strain ε. Moreover, if the integrals $\int f_\sigma(\varepsilon)d\varepsilon$ and $\int \varepsilon f_\sigma(\varepsilon)d\varepsilon$ are known in advance then Eq. (9) can be applied directly.

It should be also emphasized that there are two equations and two unknown quantities in Eqs. (7) or (9) – maximum strain ε_{max} and the position of the neutral axis ζ if $\beta = \zeta/\varepsilon_{max}$, the minimum strain ε_{min} and ζ if $\beta = (\zeta - h)/\varepsilon_{min}$, and the curvature κ and ζ if $\beta = 1/\kappa$. Thus, system (7) is solvable.

The solution of Eqs. (7) or (9) depends on the choice of an independent variable. If it is the bending moment M, then Eqs. (7) or (9) should be solved simultaneously to obtain parameters ζ and ε_{min}, or ζ and κ. If the curvature κ, or the extreme strain ε_{max}, or ε_{min} are chosen as an independent variable, then to obtain an unknown ζ, it is enough to solve only the first equation $N = 0$ in system (9). In the last case, the bending moment M can be calculated independently of the first Eq. $N = 0$ in (9).

If the stress–strain relationship of the layer, which contains a neutral axis, is different in compression and in tension, then Eqs. N and M in (9) may be expressed as follows:

$$N = \beta\left(\sum_{i=1}^{k-1} b_i \int_{\varepsilon_{i-1}}^{\varepsilon_i} f_{\sigma,i}(\varepsilon)d\varepsilon + b_k \int_{\varepsilon_{k-1}}^{0} f_{\sigma,k}(\varepsilon)d\varepsilon + b_k \int_{0}^{\varepsilon_k} f_{\sigma,k}(\varepsilon)d\varepsilon + \sum_{i=k+1}^{n} b_i \int_{\varepsilon_{i-1}}^{\varepsilon_i} f_{\sigma,i}(\varepsilon)d\varepsilon\right) = 0 \tag{11}$$

$$M = \beta^2\left(\sum_{i=1}^{k-1} b_i \int_{\varepsilon_{i-1}}^{\varepsilon_i} \varepsilon f_{\sigma,i}(\varepsilon)d\varepsilon + b_k \int_{\varepsilon_{k-1}}^{0} \varepsilon f_{\sigma,k}(\varepsilon)d\varepsilon + b_k \int_{0}^{\varepsilon_k} \varepsilon f_{\sigma,k}(\varepsilon)d\varepsilon + \sum_{i=k+1}^{n} b_i \int_{\varepsilon_{i-1}}^{\varepsilon_i} \varepsilon f_{\sigma,i}(\varepsilon)d\varepsilon\right) \tag{12}$$

where k is the number of the layer which contains neutral axis (Fig. 1).

3. Object of the study

Let us investigate the stress–strain state of the three-layered T-shaped cross section (Fig. 2). Let the flange of the cross section be made out of reinforced concrete and the web be made out of timber. Additionally, let the wooden web be strengthened by an FRP layer at the bottom of the cross section. The parabolic

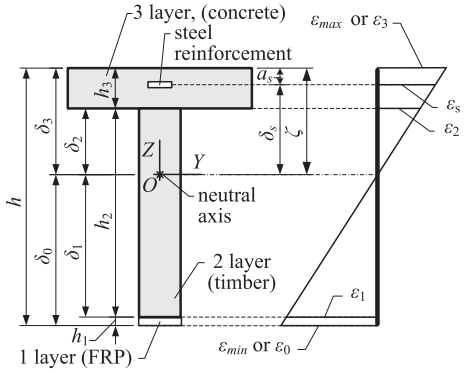

Fig. 2. Timber–concrete T cross section and distribution of the strain through its depth.

stress–strain diagram with a descending branch for short-term loading concrete, according to MC 90 [23], was used. The linear elastic perfectly plastic stress–strain relationship was adopted for steel reinforcement and linear elastic stress–strain relationship was taken for the timber and the FRP, respectively.

According to MC 90 [23], the parabolic stress–strain relationship for concrete in compression is as follows:

$$f_{\sigma,c}(\varepsilon) = \begin{cases} f_{\sigma,c,I}(\varepsilon), & \text{if } \varepsilon \leqslant \varepsilon_{c,lim} \\ f_{\sigma,c,II}(\varepsilon), & \text{if } \varepsilon > \varepsilon_{c,lim} \end{cases} \tag{13}$$

where functions $f_{\sigma,c,I}(\varepsilon)$ and $f_{\sigma,c,II}(\varepsilon)$ are given in (14) and (17), respectively.

When concrete strain varies within the range $0 \leqslant \varepsilon \leqslant \varepsilon_{c,lim}$, then $f_{\sigma,c,I}(\varepsilon)$ is as follows:

$$f_{\sigma,c,I}(\varepsilon) = f_{cm} \frac{\frac{E_{ci}}{E_{c1}}\frac{\varepsilon}{\varepsilon_{c1}} - \left(\frac{\varepsilon}{\varepsilon_{c1}}\right)^2}{1 + \left(\frac{E_{ci}}{E_{c1}} - 2\right)\frac{\varepsilon}{\varepsilon_{c1}}} \tag{14}$$

where f_{cm} is mean values of the concrete cylinder compressive strength, ε is the compressive strain of the concrete while ε_{c1} is its strain corresponding to the maximal stresses. According to MC 90 [23], ε_{c1} is the same for all classes of concrete and $\varepsilon_{c1} = 2.2 \times 10^{-3}$. In Eq. (14) E_{c1} is a secant modulus of the concrete, $E_{c1} = f_{cm}/\varepsilon_{c1}$, and E_{ci} is an initial tangent modulus of the concrete, i.e. $E_{ci} = df_{\sigma,c,I}(\varepsilon)/d\varepsilon|_{\varepsilon=0}$. According to MC 90 [23], E_{ci} is as follows:

$$E_{ci} = 2.15 \cdot 10^{10}(f_{cm}/10^7)^{1/3} \tag{15}$$

where the dimensions of the f_{cm} and E_{ci} are in Pa and GPa, respectively.

The dependence (14) holds as long as $\varepsilon \leqslant \varepsilon_{c,lim}$. The strain $\varepsilon_{c,lim} > \varepsilon_{c1}$, and $\varepsilon_{c,lim}$ corresponds to the stress $0.5 f_{cm}$. In MC 90 [23], there are given values of the $\varepsilon_{c,lim}$ for the eight classes of the concrete and a relationship for $\varepsilon_{c,lim}$ is also given. The strains $\varepsilon_{c,lim}$ at the stress $0.5 f_{cm}$ can be calculated by solving Eq. (14) with respect to the strain ε by equating $f_{\sigma,c,I}(\varepsilon_{c,lim}) = 0.5 f_{cm}$. Eq. (14) can be rearranged into quadratic equation, whose two solutions with respect to the strain ε are as follows:

$$\varepsilon = \frac{-b \pm \sqrt{D}}{2a} \tag{16}$$

where the coefficients are following: $a = f_{cm}/\varepsilon_{c1}{}^2$, $b = E_{ci}(\sigma_c/f_{cm} - 1) - 2\sigma_c/\varepsilon_{c1}$, and $D = b_2 - 4a\sigma_c$ is the discriminant, σ_c is the stresses of concrete. The positive sign before $\sqrt{D}$ corresponds to descending part of the stress–strain diagram (when $\varepsilon_{c,1} < \varepsilon \leqslant \varepsilon_{c,lim}$), while the negative sign corresponds to the rising part of the diagram (when $0 \leqslant \varepsilon \leqslant \varepsilon_{c,1}$). Thereby, to calculate the limit strain $\varepsilon_{c,lim}$

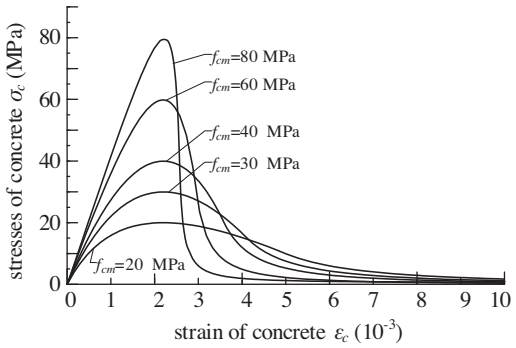

Fig. 3. Stress–strain diagram for compressive concrete according to MC90.

the positive sign has to be applied in (16) before $\sqrt{D}$ and concrete stresses σ_c has to be equated to $0.5 f_{cm}$.

In the case when concrete strain $\varepsilon > \varepsilon_{c,lim}$, the stress–strain relationship of compressive concrete can be described according to MC 90 [23] as follows:

$$f_{\sigma,c,II}(\varepsilon) = \frac{f_{cm}}{\left[\frac{\varepsilon_{c1}\xi}{\varepsilon_{c,lim}} - \frac{2\varepsilon_{c1}^2}{\varepsilon_{c,lim}^2}\right]\frac{\varepsilon^2}{\varepsilon_{c1}^2} + \left[\frac{4\varepsilon_{c1}}{\varepsilon_{c,lim}} - \xi\right]\frac{\varepsilon}{\varepsilon_{c1}}} \tag{17}$$

where ξ is

$$\xi = \frac{4\left[\left(\frac{\varepsilon_{c,lim}}{\varepsilon_{c1}}\right)^2\left(\frac{E_{ci}}{E_{c1}} - 2\right) + 2\frac{\varepsilon_{c,lim}}{\varepsilon_{c1}} - \frac{E_{ci}}{E_{c1}}\right]}{\left[\frac{\varepsilon_{c,lim}}{\varepsilon_{c1}}\left(\frac{E_{ci}}{E_{c1}} - 2\right) + 1\right]^2} \tag{18}$$

The full stress–strain diagram for compressive concrete, according to the formulas (14), (17), and (18), is shown in Fig. 3.

We assume that the linear elastic stress–strain relationships for timber and FRP are as follows:

$$f_{\sigma,j}(\varepsilon) = \varepsilon E_j, \quad j \in \{w, FRP\} \tag{19}$$

where ε and E_i are the strain and the elastic modulus of the timber and FRP, respectively.

It should be noted that, in general, the behaviour of timber is different in compression and in tension. The stress–strain relationship for timber under tension may be assumed as linear elastic while the nonlinear relationship is preferable for the compression timber [26,27]. However, some investigators also use the nonlinear diagram for tension timber [18]. In the present article the properties of the layers are chosen in such a way that neutral axis would be in the 2nd layer (timber web), that is $h_3 \leqslant \zeta \leqslant (h - h_1)$. Consequently, the concrete layer is fully in compression. Since the stiffness of the 2nd layer is bigger than the stiffness of the 1st layer the position of the neutral axis is near the connections of the layers. Therefore, the tension strain of timber is not big and the assumption about the linear elastic stress–strain relationship for compressive timber is valid.

The linear elastic perfectly plastic relationship was assumed for steel reinforcement:

$$f_{\sigma,s}(\varepsilon) = \begin{cases} \varepsilon E_s, & \text{if } \varepsilon E_s \leqslant f_y \\ f_y, & \text{if } \varepsilon E_s > f_y \end{cases} \tag{20}$$

where E_s and f_y are elastic modulus of reinforcement and its yield point.

Following the mentioned assumptions, Eqs. (11) and (12) are as follows:

$$N = \beta\left(b_1\int_{\varepsilon_0}^{\varepsilon_1} f_{\sigma,FRP}(\varepsilon)d\varepsilon + b_2\int_{\varepsilon_1}^{\varepsilon_2} f_{\sigma,w}(\varepsilon)d\varepsilon + b_3\int_{\varepsilon_2}^{\varepsilon_3} f_{\sigma,c}(\varepsilon)d\varepsilon\right) + A_s f_{\sigma,s}(\varepsilon) = 0 \tag{21}$$

$$N = \beta^2\left(b_1\int_{\varepsilon_0}^{\varepsilon_1} \varepsilon f_{\sigma,FRP}(\varepsilon)d\varepsilon + b_2\int_{\varepsilon_1}^{\varepsilon_2} \varepsilon f_{\sigma,w}(\varepsilon)d\varepsilon + b_3\int_{\varepsilon_2}^{\varepsilon_3} \varepsilon f_{\sigma,c}(\varepsilon)d\varepsilon\right) + A_s f_{\sigma,s}(\varepsilon)\delta_s = 0 \tag{22}$$

where A_s is the area of the cross section of the reinforcement, δ_s is the distance from the neutral axis to the centroid of the reinforcement (Fig. 2). The integration limits ε_i, $i \in \{0,1,2,3\}$, in (21) and (22) are as follows:

$$\varepsilon_0 = \frac{1}{\beta}(\zeta - h) = \varepsilon_{min}, \quad \varepsilon_1 = \frac{1}{\beta}(\zeta - h_2 - h_3),$$
$$\varepsilon_2 = \frac{1}{\beta}(\zeta - h_3) \quad \text{and} \quad \varepsilon_3 = \frac{1}{\beta}\zeta = \varepsilon_{max} \tag{23}$$

Since the stress–strain dependence of the concrete is a piecewise function (13), then the integrand $f_{\sigma,c}(\varepsilon)$ in the integrals $\int_{\varepsilon_2}^{\varepsilon_3} f_{\sigma,c}(\varepsilon)d\varepsilon$ and $\int_{\varepsilon_2}^{\varepsilon_3} \varepsilon f_{\sigma,c}(\varepsilon)d\varepsilon$ of Eqs. (21) and (22) equals $f_{\sigma,c,I}(\varepsilon)$ when $\varepsilon_3 \leqslant \varepsilon_{c,lim}$ and $f_{\sigma,c,II}(\varepsilon)$ when $\varepsilon_2 > \varepsilon_{c,lim}$, respectively, here $\varepsilon_3 = \varepsilon_{max}$. When $\varepsilon_2 \leqslant \varepsilon_{c,lim}$ and $\varepsilon_3 > \varepsilon_{c,lim}$, then:

$$\int_{\varepsilon_2}^{\varepsilon_3} f_{\sigma,c}(\varepsilon)d\varepsilon = \int_{\varepsilon_2}^{\varepsilon_{c,lim}} f_{\sigma,I}(\varepsilon)d\varepsilon + \int_{\varepsilon_{c,lim}}^{\varepsilon_3} f_{\sigma,I}(\varepsilon)d\varepsilon$$
$$\int_{\varepsilon_2}^{\varepsilon_3} \varepsilon f_{\sigma,c}(\varepsilon)d\varepsilon = \int_{\varepsilon_2}^{\varepsilon_{c,lim}} \varepsilon f_{\sigma,I}(\varepsilon)d\varepsilon + \int_{\varepsilon_{c,lim}}^{\varepsilon_3} \varepsilon f_{\sigma,II}(\varepsilon)d\varepsilon \tag{24}$$

For the FRP and the timber layers the integrals of Eqs. (21) and (22) are following:

$$\int_a^b f_{\sigma,j}(\varepsilon)d\varepsilon = \int_a^b E_j\varepsilon d\varepsilon = 1/2E_j(b^2 - a^2) \tag{25}$$

$$\int_a^b \varepsilon f_{\sigma,j}(\varepsilon)d\varepsilon = \int_a^b E_j\varepsilon^2 d\varepsilon = 1/3E_j(b^3 - a^3) \tag{26}$$

where $j \in \{w, FRP\}$.

For concrete layer, the integrals of Eqs. (21) and (22) are following:

$$\int_a^b f_{\sigma,c,I}(\varepsilon)d\varepsilon = f_{cm}\left(\frac{(b-a)v_0^2}{v_1^2} - \frac{1}{2}\frac{f_{cm}(b^2 - a^2)}{\varepsilon_{c1}v_1}\right) - \frac{f_{cm}^2\varepsilon_{c1}v_0^2}{v_1^3} \times \ln\left(\frac{v_1 b + f_{cm}\varepsilon_{c1}}{v_1 a + f_{cm}\varepsilon_{c1}}\right) \tag{27}$$

where $v_0 = 1.05E_{cm}\varepsilon_{c1} - f_{cm}$ and $v_1 = 1.05E_{cm}\varepsilon_{c1} - 4f_{cm}$,

$$\int_a^b f_{\sigma,c,II}(\varepsilon)d\varepsilon = \frac{f_{cm}\varepsilon_{c,lim}\varepsilon_{c1}}{\xi\varepsilon_{c,lim} - 4\varepsilon_{c1}} \ln\left(\frac{a(v_3 b + v_2)}{b(v_3 a + v_2)}\right) \tag{28}$$

where $v_2 = 4\varepsilon_{c,lim}\varepsilon_{c1} - \xi\varepsilon_{c,lim}^2$ and $v_3 = \xi\varepsilon_{c,lim} - 2\varepsilon_{c1}$,

$$\int_a^b \varepsilon f_{\sigma,c,I}(\varepsilon)d\varepsilon = \frac{f_{cm}^3\varepsilon_{c1}^2 v_0^2 \ln\left(\frac{f_{cm}\varepsilon_{c1} - v_4 b}{f_{cm}\varepsilon_{c1} - v_4 a}\right)}{v_4^4} + \frac{f_{cm}v_0^2(v_4\varepsilon_{c1}(b^2 - a^2) + 2f_{cm}\varepsilon_{c1}^2(b-a))}{2v_4^3\varepsilon_{c1}} + \frac{f_{cm}^2(b^3 - a^3)}{3v_4\varepsilon_{c1}} \tag{29}$$

where $v_4 = 2f_{cm} - 1.05E_{cm}\varepsilon_{c1}$,

$$\int_a^b \varepsilon f_{\sigma,c,II}(\varepsilon)d\varepsilon = \frac{1}{v_3}f_{cm}\varepsilon_{c,lim}^2\varepsilon_{c1} \ln\left(\frac{v_3 b + v_2}{v_3 a + v_2}\right) \tag{30}$$

where v_2 and v_3 are given in Eq. (28). In Eqs. (27)–(30) the limits of the integration a and b are strains and $a \leqslant b$.

It should be noted that the stress–strain relationship for compressive concrete (14) according to MC 90 [23] and EC2 [25] is really the same. Only the notations are different. According to EC2 [25] in (14) $E_{c1} = 1.05\,E_{cm}$. Also values of the strain ε_{c1} are different for some classes of the concrete. Therefore, the obtained integrals (27) and (29) can be used for calculation according to the EC2 [25] requirements.

4. The solution of the equations system

Both Eqs. (21) and (22) together with (23), (25), (26), (27), (28), (29), and (30) are nonlinear. They should be solved numerically. These equations may have one, two and even three roots. It should be emphasised that all three roots may be actual. For example, if ζ_i, $i \leqslant 3$, is one of the roots of Eqs. (21) and (22) then the case is possible when $h_3 \leqslant \zeta_i \leqslant (h - h_1)$. Therefore, there can be difficulties in distinguishing the required root among others. One way how to do it is to solve Eqs. (21) and (22) at the beginning of the loading or deformation, because there is only one actual root when ε_{min}, ε_{max}, κ, or M tend to zero. Gradual increasing one of these variables leads to gradual variation of the actual solution. Then it is possible to identify the required root according to its closeness to the previous value. However, some difficulties still remain when the actual root changes discontinuously. If at the jump Eqs. (21) and (22) have only one actual root, then the given rule can be applied to the further roots as well. In the present article Eqs. (21) and (22) were solved with the program Maple.

5. Analysis of the results

In this chapter the results of the analysis of the behaviour of the TCC cross section under the bending moment are given. The influence of the cross section geometrical parameters, materials parameters, steel reinforcement and FRP on the deformation parameters was investigated. To illustrate this influence the analysis was performed using five types of cross sections (Table 1): the first three types are TCC cross sections without any steal and FRP reinforcement, the fourth and the fifth types are cross sections only with steal or only with FRP reinforcement.

The deformation of the cross section is characterized with four parameters: the bending moment M, extreme strains ε_{min} and ε_{max}, and the position of the neutral axis ζ. For more convenience the extreme strains of the timber and concrete layers are referred to by the symbols $\varepsilon_{min,w}$ and $\varepsilon_{max,c}$, that is $\varepsilon_{min,w} = \varepsilon_1$ for the timber layer and $\varepsilon_{max,w} = \varepsilon_3$ for the concrete layer. The extreme strains $\varepsilon_{min,w}$ and $\varepsilon_{max,c}$ as well as the curvature κ corresponding to the local maximum of the bending moment M_{max} were also investigated. In this case they are denoted as ε^*_{min}, ε^*_{max} and κ^*. For more clarity the ε^*_{min} and ε^*_{max} are depicted in Fig. 6. In Fig. 4, Fig. 10 and Fig. 11, the vertical dotted lines and diamond-like markers, on the abscissa, denote the values of the curvature κ^*.

In order to model the behaviour of the cross section under the load, three variables can be chosen as independent in Eqs. (21) and (22): extreme strains ε_{max}, ε_{min}, and curvature κ. It is evident that deflection is related unambiguously to curvature; therefore, there is natural reason to choose the curvature as an independent variable to analyze the stress–strain state of the cross section. It should be emphasized that the bending moment as an independent variable is not as convenient as the curvature κ because one value of M may correspond to two values of each strain $\varepsilon_{min,w}$ or $\varepsilon_{max,c}$. Thus, in the present article the curvature κ is taken as an independent variable.

In the Table 1 the concrete properties are characterized only by its mean strength f_{cm}. The initial tangent modulus of elasticity E_{ci} of the concrete can be obtained by Eq. (15). It was also assumed that the modulus of the elasticity E_{FRP} of the FRP and its strength f_{FRP} are as follows: $E_{FRP} = 130$ GPa and $f_{FRP} = 1750$ MPa. These values were taken for carbon FRP according to [28]. The class of the steel reinforcement was taken B500 whose yield point $f_s = 500$ MPa. In the present analysis the stresses and strains of timber were not restricted, that is, the strength of the timber was always taken bigger than the absolute value of the maximum stresses.

Due to a small diameter of the reinforcing steel bars and small thickness of the FRP layer the amount of these reinforcements were represented in terms of reinforcement ratios ρ_s and ρ_{FRP} for steel and FRP reinforcement, respectively:

$$\rho_j = \frac{A_j}{b_3 h_3 + (b_2 h_2) E_w / E_{ci}}, \quad j \in \{FRP, s\} \tag{31}$$

where A_s and A_{FRP} are areas of the steel and FRP reinforcement, respectively.

The width of the 1st FRP layer is the same as the width of the 2nd timber layer. The position of the reinforcement within 3rd concrete layer was equal to $a_s = 5$ cm (Fig. 2).

5.1. Analysis of the timber–concrete cross section

Let us start the analysis from the TCC cross section without any steel and FRP reinforcements. The cross section is I type (Table 1). Fig. 4 shows that the dependences of the parameters of the deformations ζ, M, ε_{min} and ε_{max} with respect to the curvature κ may have jump discontinuity when $\kappa \geqslant \kappa^*$ (descending branch on κ–M graph). Where κ^* is the curvature corresponding to the local maximum of the bending moment M_{max}. These dependences may be continuous for the cross sections with low strength concrete and low ratio of the thickness h_3/h_2 of the layers. The decrease of the stresses of low strength concrete, when $\varepsilon_c > \varepsilon_{c1}$, is not as sharp as of higher strength concrete. It indicates that the discontinuities appear due to the sharp descending branch of the adopted stress–strain diagram of the concrete. These discontinuities are indicated clearly for high strength concrete in Fig. 4. Mathematically, the discontinuities can be treated as follows. If Eqs. (21) and (22) are solved with respect to one of the variables ζ, M, ε_{min}, ε_{max}, then the discontinuities in Fig. 4 point out that Eqs. (21) and (22) do not have solution in certain interval. Consequently, the dependence of the curvature κ on ζ, M, ε_{min} or ε_{max} is not defined within certain interval. Physically, these discontinuities should correspond to abrupt redistribution of the strains state of the cross section – abrupt decrease of the bending moment M and abrupt increase of the curvature or deflection. In addition, this phenomenon may be treated as sudden partial fracture of the whole cross section or fracture of the concrete due to sudden increase of the strain $\varepsilon_{max,c}$.

5.1.1. Position of the neutral axis

Fig. 4a shows that the position of the neutral axis ζ increases monotonically with increasing the curvature κ and tends to $(1/2\ h_2 + h_3)$. At the beginning of the loading the concrete deforms almost elastically. It should be noted that the experimental investigation conducted by Ceccoti [6] also showed a similar tendency of the behaviour of the position of the neutral axis when the strength of concrete $f_{cm} = 30.4$ MPa. Therefore, at this stage the position of the neutral axis can be calculated according to a well known formula:

$$\zeta_{el} = \sum_{i=1}^{n} E_i S_i \Big/ \sum_{i=1}^{n} E_i A_i \tag{32}$$

where n is number of the layers, E_i is modulus of the elasticity of the ith layer, S_i and A_i are the first order moment and area of the ith layer, respectively. In this case the S_i shall be calculated with respect to the top edge of the cross section.

Table 1
Types of the used cross sections and their properties.

Type of cross section	1st Layer (FRP)		2nd Layer (timber)			Steel reinforcement		3rd Layer (concrete)		
	ρ_{FRP} (%)	E_{FRP} (GPa)	b_2 (m)	h_2 (m)	E_w (GPa)	ρ_s(%)	E_s (GPa)	b_3 (m)	h_3 (m)	f_{cm} (MPa)
I	0	–	0.2	0.4	10	0	–	0.6	0.1	Varies from 20 up to 80
II	0	–	0.2	0.4	10	0	–	0.6	0.1	40
III	0	–	$(b_3/b_2)=5$, $0\leqslant(h_3/h_2)\leqslant 0.8$		10 or 20	0	–	$(b_3/b_2)=5$, $0\leqslant(h_3/h_2)\leqslant 0.8$		Varies from 20 up to 80
IV	Varies from 0 up to 3	130	0.2	0.4	10	0	–	0.6	0.1	40
V	0	–	0.2	0.4	10	Varies from 0 up to 3	200	0.6	0.1	40

Let $\zeta = \zeta_{el}$ at the beginning of the deformation, i.e. when $\kappa \to 0$. The ζ_{el} remains the same for the interval $[0,\kappa^*]$ because ζ_{el} by (32) does not depend on the curvature κ. Then, as can be seen from this picture, ζ tends to ζ_{el} with increasing strength of the concrete as $\kappa \in [0,\kappa^*]$. When the strength of concrete is 80 MPa the ζ remains practically the same up to the discontinuity point κ^*. Consequently, the ζ may be calculated by the formula (32) when concrete strength is big enough.

5.2. Bending moment

The analysis shows that the dependence of the bending moment on the curvature κ may not have local maximum when strength of the concrete is low and (or) concrete layer thickness is small enough. The picture Fig. 4b shows that κ^* at local maximum M_{max} increase with increasing the concrete strength. Analysis also showed that κ^* increases with increasing ratio h_3/h_2.

In Fig. 5, there are depicted two kinds of the bending moments for the I type cross section: the characteristic bending moments M_k, according to the linear elastic analysis of EN 1995-1-1 [15] (Appendix B), depicted by open circles; and the bending moments according to Eqs. (21) and (22), depicted by curves. The characteristic bending moments M_k, $M_k = \kappa(EI)_{ef}$, where $(EI)_{ef}$ is effective bending stiffness according to [15], were calculated taking the position of the neutral axis according to Eq. (32) and assuming the following parameters: the slip modulus of the joint equals infinity, the strength class of the timber is C22 according to EN 338:2009 [29], then modulus of elasticity and characteristic strength of the timber $E_w = 10$ GPa and $f_w = 22$ MPa, respectively; the characteristic strength and secant modulus of the concrete $f_{ck} = f_{cm} - 8$ MP and $E_{cm} = 0.85E_{ci}$, respectively, according to recommendations of MC90 [23], where E_{ci} is given in (15). The moments M_k were calculated when either $max\{|\sigma_w|\} = f_w$ and $max\{\sigma_c\} \leqslant f_{ck}$ or $max\{|\sigma_w|\} \leqslant f_w$ and $max\{\sigma_c\} = f_{ck}$, where σ_c, σ_w, f_w and f_{ck} are stresses and characteristic strengths of the concrete and timber, respectively. As can be seen from Figs. 4 and 5 the values of M_k are much smaller than M_{max}. In addition, the dependency of M_k on concrete strength f_{cm} is weaker than the dependency of M on f_{cm} according to nonlinear analysis (Eqs. (21) and (22)). It is due to the fact that M_k is restricted mainly to low strength of the timber (except the case when $f_{cm} = 20$ MPa).

5.3. Analysis of the extreme strains $\varepsilon_{max,c}$ and $|\varepsilon_{min,w}|$

As can be seen from Fig. 4c the values of the maximum concrete stains $\varepsilon_{max,c}$ (at the top edge of the cross section) decrease with

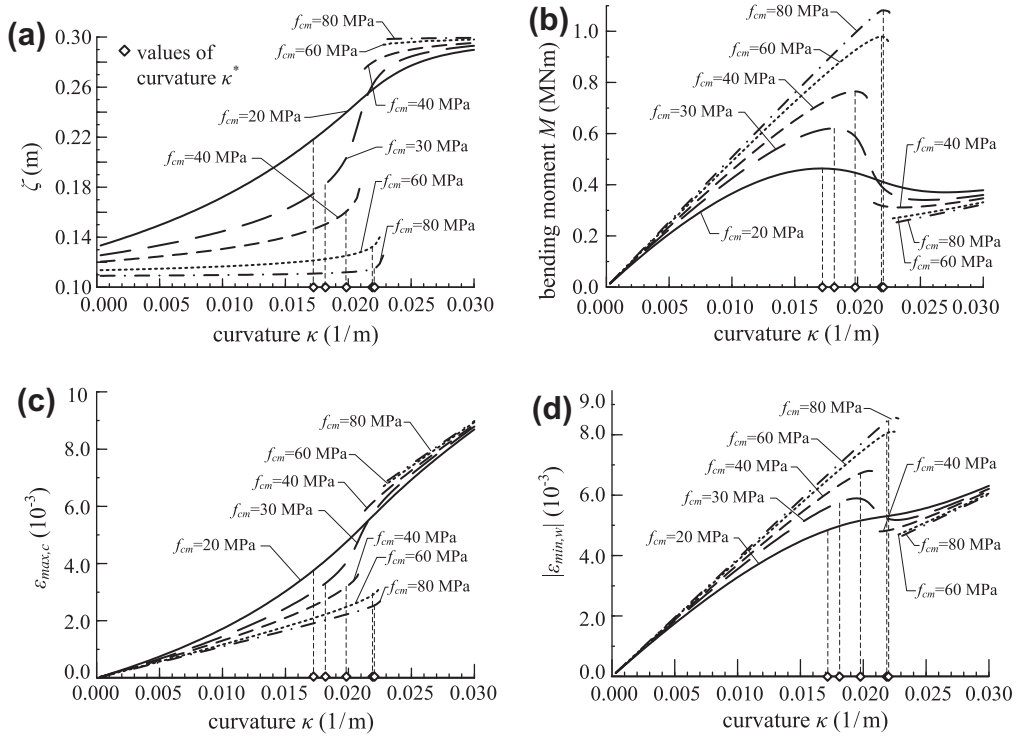

Fig. 4. The dependences of the parameters of the deformations on the curvature κ when type of the cross section is I: *a* is position of the neutral axis ζ, *b* is bending moment *M*, *c* is maximum strain $\varepsilon_{max,c}$ of the concrete and *d* is absolute values of minimum strain $|\varepsilon_{min,w}|$ of the wood.

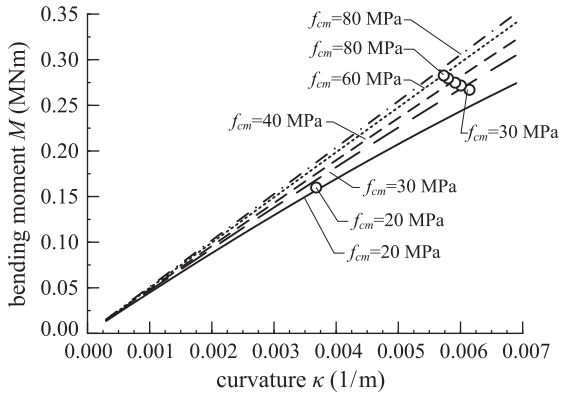

Fig. 5. The dependences of the bending moments on curvature (lines) and characteristic values of the bending moment according to linear elastic analysis of EN 1995-1-1 [15] (Appendix B) (open circles).

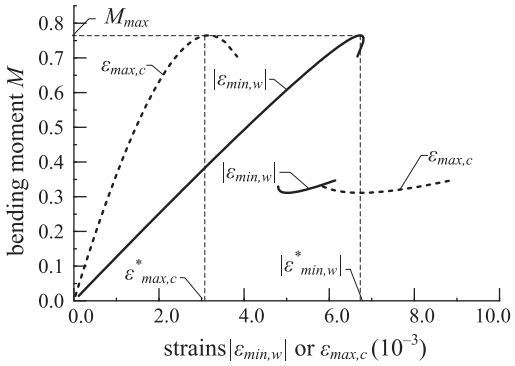

Fig. 6. The parametric curves of the strains $\varepsilon_{max,c}$ and $|\varepsilon_{min,w}|$ and the bending moments M of the II type of the cross section.

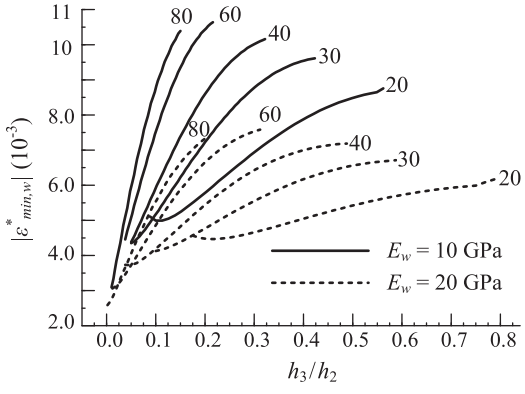

Fig. 7. The dependences of the maximum values of the strains at the local maximum M_{max} for III type cross section.

increasing strength of concrete when $\kappa \in \{0, \kappa^*\}$ and, on the contrary, the absolute minimum value of the strain $|\varepsilon_{min,w}|$ of timber (at the bottom edge of the cross section) increases with increasing strength of concrete (Fig. 4). At the point of the discontinuity the $\varepsilon_{max,c}$ increases and $|\varepsilon_{min,w}|$ decreases abruptly. The parametric curves of the strains $\varepsilon_{max,c}$ and $|\varepsilon_{min,w}|$ and the bending moments M are depicted in Fig. 6 when the type of the cross section, according to Table 1, is II.

Fig. 4 also illustrates that due to the softening of the concrete the deformation parameters ζ, M, $\varepsilon_{max,c}$, and $\varepsilon_{min,w}$ tend to the

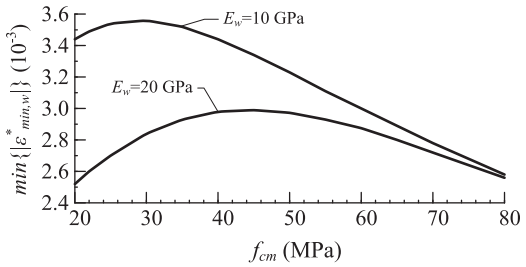

Fig. 8. The dependences of the minimum values of the minimal values of the strain of the timber on concrete strength at the local maximum M_{max}.

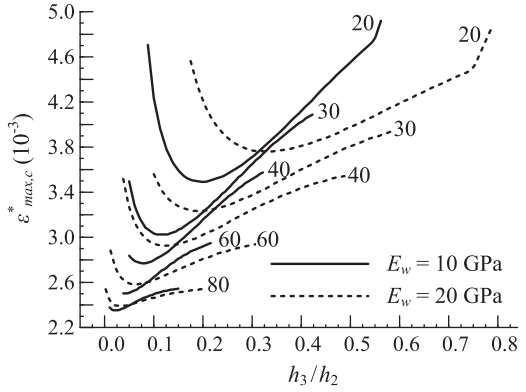

Fig. 9. The dependences of the maximal values of the strain of the concrete at the local maximum M_{max}.

Table 2
The values of the ratios of the bending moment.

f_{cm}	20	30	40	60	80
$\frac{M_{cw,lim}}{M_{max}}$	0.55	0.43	0.36	0.29	0.26
$\frac{M_{scal}}{M_{max}}$	1	0.99	0.65	–	0.9

corresponding values of the deformation parameters of the wooden cross section which is made out of only the 2nd layer (timber).

The dependences of the absolute minimum $|\varepsilon^*_{min,w}|$ and maximum $|\varepsilon^*_{max,c}|$ values of the strain corresponding to the local maximum M_{max} of the bending moment M are given in Figs. 7 and 9. The type of the cross section is III. It should be noted that the loading stage when $M = M_{max}$ can be considered as the ultimate limit state of the cross section under pure bending. The solid line depicts the strain when $E_w = 10$ GPa, and the dotted line when $E_w = 20$ GPa. The numbers beside the lines indicate the mean strength f_{cm} of concrete. The range of the ratio h_3/h_2 was taken as $[0, 0.8]$. However, the values of the $|\varepsilon^*_{max,c}|$ and $|\varepsilon^*_{min,w}|$ are depicted for those values of the ratio h_3/h_2 for which the local maximum M_{max} exits and for which the neutral axis is in the 2nd wooden layer that is while $\zeta > h_3$.

Fig. 7 illustrates that the strain $|\varepsilon^*_{min,w}|$ increases with increasing ratio h_3/h_2 and the strength of concrete f_{cm}; however, the $|\varepsilon^*_{min,w}|$ decreases with increasing modulus of elasticity of the wood E_w. The dependence of the $|\varepsilon^*_{min,w}|$ on the ratio h_3/h_2 is not strictly increasing for the low strength concrete, i.e. when $f_{cm} = 20$ MPa. It is also determined that $|\varepsilon^*_{min,w}|$ increases monotonically with increasing ratio b_3/b_2 of the widths of the layers.

Let us investigate minimum values of the $|\varepsilon^*_{min,w}|(min\{|\varepsilon^*_{min,w}|\})$ as the following limits are assumed: $(b_3/b_2) \in [1, 10]$, $(h_3/h_2) \in [0, 0.8]$, $E_w \in \{10, 20\}$ GPa, and $f_{cm} \in [20, 80]$ MPa. It should be noted that these limits correspond to the set of the cross sections that are

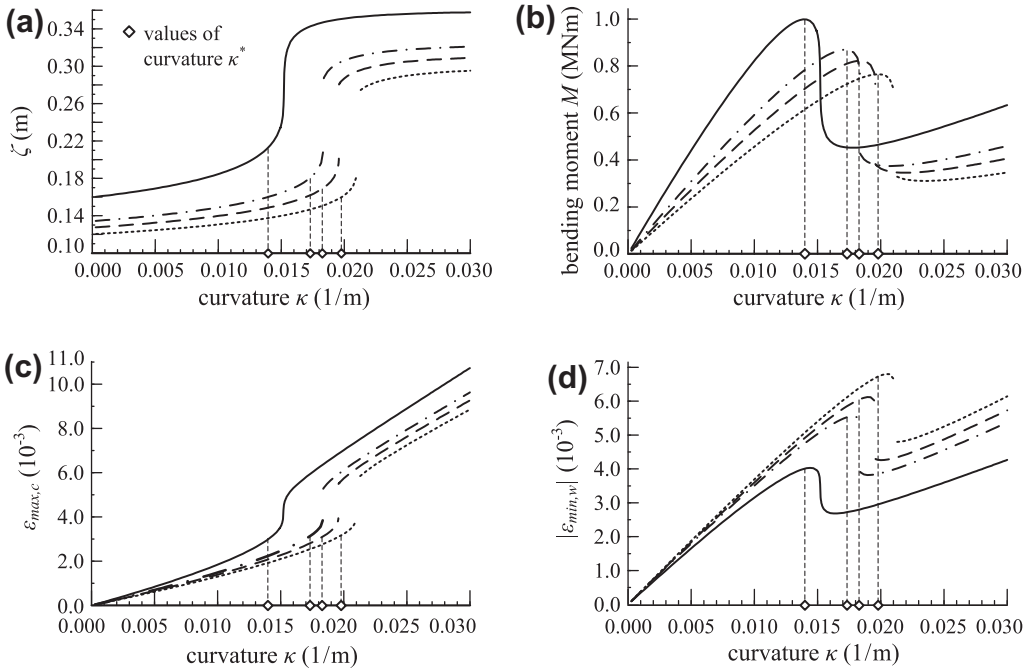

Fig. 10. The dependences of the parameters of the deformations of the IV type cross section on the curvature κ: ... when $\rho_{FRP} = 0.0\%$, – – – when $\rho_{FRP} = 0.5\%$, – · – · when $\rho_{FRP} = 1.0\%$, and – when $\rho_{FRP} = 3.0\%$.

really used in civil engineering. Since $|\varepsilon^*_{min,w}|$ decreases monotonically with decreasing of the ratio b_3/b_2, then the $min\{|\varepsilon^*_{min,w}|\}$ would be obtained if the ratio b_3/b_2 was minimal. For real structures it may be assumed that the minimal values of the b_3/b_2 equal to 1 and in our analysis it is also assumed that $b_3/b_2 = 1$. Then minimum values $min\{|\varepsilon^*_{min,w}|\}$ of the strain $|\varepsilon^*_{min,w}|$ under assumed limits are depicted in Fig. 8.

Let us compare $|\varepsilon^*_{min,w}|$ with the limit values of the wood's strain $\varepsilon_{w,lim} = E_w/f_w$ when materials properties are taken from code EN 338:2009 [29]. The properties of the wood indicated in this code are used to design wooden structures in civil engineering. According to this document, the mean values of the modulus of the elasticity of the wood varies within the interval $(7 \leqslant E_w \leqslant 20)$ GPa, while characteristic bending strength of the wood varies within the interval $(14 \leqslant f_w \leqslant 70)$ MPa, and characteristic tensile strength along the grain of the wood varies within interval $(8 \leqslant f_w \leqslant 42)$ MPa. Therefore the estimations of the minimal and maximal values of the limits strain of the wood may be as follows: $\varepsilon_{w,lim} = E_w/f_w$ is 2×10^{-3} when $E_w = 7$ GPa and 3.5×10^{-3} when $E_w = 20$ GPa, respectively. If we take into account that the design values of the strength of the solid timber are at least 1/3 smaller than the characteristic values and that the ratio $b_2/b_1 = 1$ is a very specific case for real structures, then it is possible to claim that the strains $|\varepsilon^*_{min,w}|$ of the TCC T cross section are much bigger than the limit values of wood's strain $\varepsilon_{w,lim} = E_w/f_w$. Fig. 7 illustrates it obviously because the $|\varepsilon^*_{min,w}|$ varies within the interval $[4.99 \times 10^{-3}, 6.17 \times 10^{-3}]$ when $E_w = 20$ GPa and $f_{cm} = 20$ MPa, respectively. And these values are minimum values over assumed limits; (b_3/b_2), (h_3/h_2), E_w. The following conclusion can be formulated in terms of stress: the stresses of the wood at local maximum of the bending moment are much bigger than the strength of wood.

The given comparison could seem incorrect because the strength of the concrete was taken as mean value and the limit deformation of the timber were determined by taking the characteristics or design values of the wood. That is, the quantiles of the strength of the concrete and wood were different. However, the proposed conclusion remains valid because the inequality $\varepsilon_{w,lim} \ll |\varepsilon^*_{min,w}|$ is also valid for low strength concrete, which may be treated as the actual or the design strength of the concrete.

The dependences of the maximal strain of the concrete $\varepsilon^*_{max,c}$ on the ratio h_3/h_2 at ultimate state for cross section of III type are depicted in Fig. 9. The picture shows that $\varepsilon^*_{max,c}$ decreases with increasing concrete strength f_{cm}. The $\varepsilon^*_{max,c}$ has an absolute minimum within the interval h_3/h_2 in which $\varepsilon^*_{max,c}$ is defined and maximum at the maximum value of the ratio h_3/h_2 of the domain of definition of the $\varepsilon^*_{max,c}$.

According to the design codes the maximum absolute values of the compressive strain of the concrete shall be limited. For example, according to EC2 [25] for a parabola stress–strain diagram with a descending branch the ultimate values of the compressive strain ε_{cu1} are as follows: 3.5×10^{-3} when $f_{cm} \leqslant 58$ MPa, 3.36×10^{-3} when $f_{cm} = 60$ MPa and 2.82×10^{-3} when $f_{cm} = 80$ MPa. According to code ACI 318 [30] the ultimate values of compressive strain of the concrete in bending members is 3.0×10^{-3}. Fig. 9 shows that for the given cross section ε_{cu1} does not exceed only when $f_{cm} \geqslant 60$ MPa. If the strain of the timber is restricted by the limit $\varepsilon_{w,lim} = E_w/f_w$, then maximal strain of concrete $\varepsilon_{max,c}$ is small enough in comparison with the strain ε_{c1} at the maximal stress $\sigma = f_{cm}$. Therefore, it can be assumed that the behaviour of the concrete is linear elastic in the considered interval of the concrete strain, especially for higher classes of the concrete. The analysis of the position ζ of the neutral axis confirms that assumption. Both reasons allow us to think that linear elastic approach is suitable enough for calculation of the TCC T cross sections.

Let us compare the maximum bending moment M_{max} with bending moments $M_{\varepsilon w,lim}$ and $M_{\varepsilon cu1}$. Here $M_{\varepsilon w,lim}$ is a bending moment when $|\varepsilon_{min,w}| = \varepsilon_{w,lim} = E_w/f_w$ and $M_{\varepsilon cu1}$ is a bending moment when $\varepsilon_{max,c} = \varepsilon_{cu1}$, respectively. In this case it is assumed that the strength class of the timber is C22 according to EN 338:2009 [29]. Then $E_w = 10$ GPa, $f_w = 22$ MPa and $\varepsilon_{w,lim} = 2.2 \times 10^{-3}$. The values of the ε_{cu1} are taken according to EC2 [25] and $\varepsilon_{cu1} = 3.5 \times 10^{-3}$. The cross section is I type. The ratios of the bending moments are given in the Table 2. It should be noted that the ratio $M_{\varepsilon cu1}/M_{max}$ is absent in the Table 2 for value $f_{cm} = 60$ MPa, because the bending

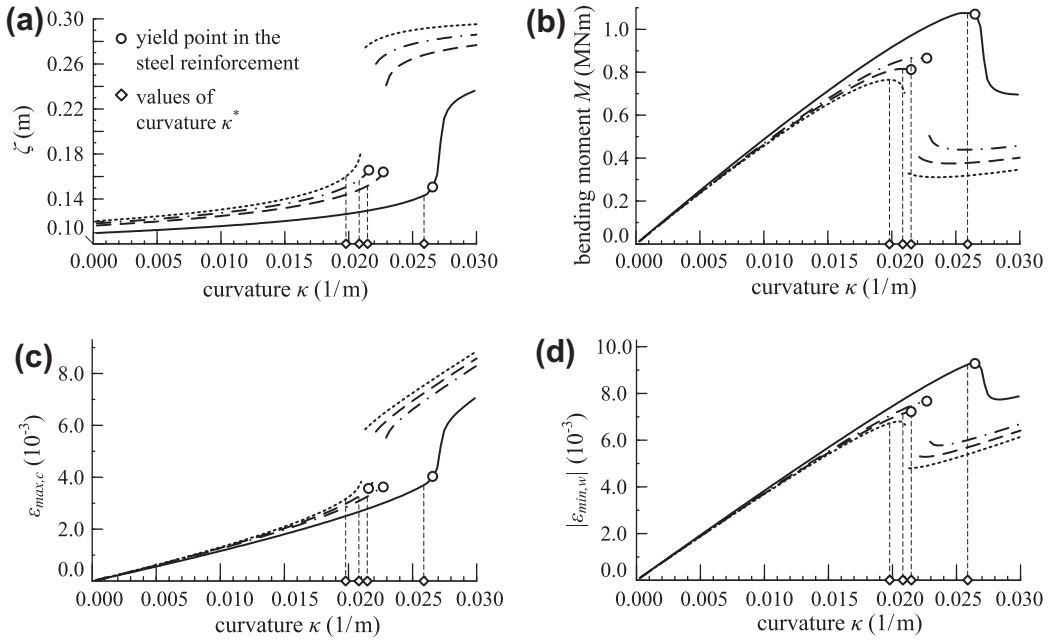

Fig. 11. The dependences of the parameters of the deformations of the V type cross section on the curvature κ: ... when $\rho_s = 0.0\%$, – – – when $\rho_s = 0.5\%$, – · – · when $\rho_s = 1.0\%$, – when $\rho_s = 3.0\%$.

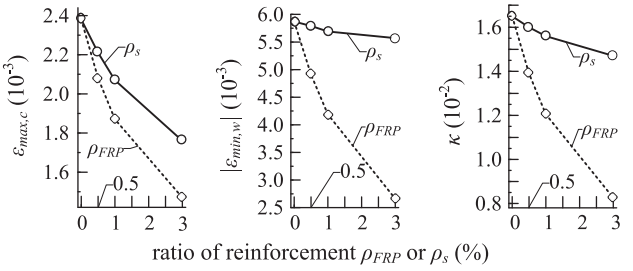

Fig. 12. The dependences of $\varepsilon_{max,c}$, $|\varepsilon_{min,w}|$ and κ on the ratio of the reinforcement of the compression or tension zones, respectively for IV and V types of the cross sections when $M = 0{,}7$ MNm, —○— and ···○··· refer to the cross section with compression steel or tension FRP reinforcement respectively.

moment at ε_{cu1} is not defined, actually the concrete maximum strains $\varepsilon_{c,max}$ at M_{max} are less than ε_{cu1}.

Table 2 indicates clearly that the bearing capacity of the TCC *T* cross section is restricted mainly due to low strength of the wood. Similar conclusion was made in analysis of characteristic bending moment M_k (Section 5.2). The ratio $M_{\varepsilon w,\mathrm{lim}}/M_{max}$ decreases with increasing f_{cm}. Therefore, it is not worth using the high strength concrete for TCC *T* cross section. To increase bearing capacity of the cross section the tension zone should be strengthened. There are many possibilities how to do it. One of them is an externally bonded FRP. The concrete layer should be reinforced with steel reinforcement as well.

5.4. Analysis of the reinforced timber–concrete cross section

In order to illustrate the influence of the steel reinforcements and FRP on the stress–strain state of the cross-section, two types of the reinforced cross sections were chosen: IV and V (Table 1, Fig. 2). The dependences of the deformation parameters on the curvature κ are depicted in Figs. 10 and 11. The open circles in Fig. 11 denote the values of the curvature κ at which yield point in the compression reinforcement was reached.

It is evident that at the same bending moment the values $|\varepsilon_{min,w}|$, $\varepsilon_{max,c}$, and κ decrease with increasing amount of the compression or tension reinforcement. However, as can be seen from Fig. 10 and Fig. 11 the character of the dependences of the deformations parameters on the curvature κ depends on the reinforcement kind. The FRP reinforcement of the tension zone increases ζ and $\varepsilon_{max,c}$ and decreases $|\varepsilon_{min,w}|$ while steel reinforcement of the compression zone decreases ζ and $\varepsilon_{max,c}$ and increases $|\varepsilon_{min,w}|$ (Fig. 10) in respect to the curvature κ. Moreover, the FRP reinforcement of the tension zone reduces $|\varepsilon^*_{min,w}|$ and κ^* and increases $\varepsilon^*_{max,c}$ (Fig. 10) while steel reinforcement increases $|\varepsilon^*_{min,w}|$ and κ^* and reduces $\varepsilon^*_{max,c}$ (Fig. 11). Consequently, at the maximal bending moment M_{max}, the reinforcement of the tension zone reduces the deflection of the beam, while reinforcement of the compression zone increases one.

The analysis has also shown that κ, $\varepsilon_{max,c}$ and $|\varepsilon_{min,w}|$ are bigger for cross section with reinforcement of the compression concrete zone than for cross section with reinforcement of a tension zone at the same bending moment. This statement is valid even if the amount and the type of the reinforcements of both zones are the same. As a consequence, the deflection of the TCC *T* cross section bending member with reinforcement of the tension zone is less than deflections of the same member but with reinforcement of the compression zone. Due to these observations, we can state that reinforcement of the tension zone is more effective than reinforcement of the compression zone for considered cross-sections.

The reason for the above given phenomenon is the difference in the sizes of the compression and the tension zones. The compression zone is smaller than the tension one, that is, $\zeta < |h - \zeta|$. Therefore, the distance between the neutral axis and the resultant of the compression reinforcement is smaller than the distance between the neutral axis and the resultant of the tension reinforcement.

This statement may be illustrated using Fig. 10 and Fig. 11. Even though the modulus of the elasticity of the steel was chosen higher than FRP the deformation parameters κ, $\varepsilon_{max,c}$ and $|\varepsilon_{min,w}|$ are bigger for the cross section with compression steel reinforcement than with tension FRP reinforcement.

The dependences of the $\varepsilon_{max,c}$, $|\varepsilon_{min,w}|$, and κ on the ratio of the reinforcement of the compression or tension zones are depicted in Fig. 12 when bending moment $M = 0.7$ MNm. The cross sections are IV and V types. The solid and dotted lines indicate the cases when the cross section is reinforced only with compression (Vth type of the cross section) or tension reinforcement (IVth type of the cross section), respectively.

It should be noted that strengthening of the cross-sections with externally bonded FRP is not convenient and desirable for new structures due to more complicated technologies and additional expenditures. FRP is still expensive material in comparison with steel reinforcement, wood or concrete. However, externally bonded FRP can be used to strengthen and retrofit the existing structures. The present analysis showed this possibility.

As can be seen from Fig. 12, the $\varepsilon_{max,c}$, $|\varepsilon_{min,w}|$ and κ decrease with increasing reinforcement ratios ρ_s and ρ_{FRP}. However, the decrease is more sudden for the cross section with tension reinforcement than with the compression reinforcement.

Finally, we notice that due to the fact that the stress–strain relationship for compressive concrete, according to MC 90 [23] and EC2 [25], is really the same; there are only small differences in E_{ci} and ε_{c1}. Then, the conducted analysis is also valid for TCC *T* cross sections when the requirements for concrete are according to EC2 [25].

6. Conclusions

The performed analysis showed that the bearing capacity of the TCC *T* cross section is restricted mainly due to low strength of the timber and the bearing capacity of the concrete layer is not utilized fully. To improve the utilization of the bearing capacity of the concrete layer, the reinforcement of the tension zone of the timber is necessary. The analysis showed that TCC *T* cross section may be calculated as linear elastic neglecting the nonlinear behaviour of the concrete. The maximal strain of the concrete of the cross section at limit state are usually higher than the ultimate compressive strain of the concrete according to the design codes EC2 and ACI 318, especially for low strength concrete. The tension reinforcement is more effective than compression reinforcement. The former reduces the curvature and the absolute values of the strains of the tension and compression zones more than reinforcement of the compression zone. Analysis showed that the tension reinforcement reduces the curvature and the absolute value of the strain of the tension zone and increases the absolute value of the strain of the compression zone at the limit state. The compression reinforcement increases the curvature and the absolute value of the strain of the tension zone and decreases the absolute value of the strain of the compression zone at a limit state.

References

[1] Yeoh D, Fragiacomo M, De Franceschi M, Boon KH. State of the art on timber–concrete composite structures: literature review. J Struct Eng 2011;137(10):1085–95.
[2] Gutkowski RM, Balogh J, To LG. Finite-element modeling of short-term field response of composite wood–concrete floors/decks. J Struct Eng 2010;136(6):707–14.
[3] Gutkowski R, Brown K, Shigidi A, Natterer J. Laboratory tests of composite wood–concrete beams. Constr Build Mater 2008;22(6):1059–66.
[4] Schäfers M. Development of adhesive bonded timber-uhpc composites – experimental and theoretical investigations. In: Proceedings of the 11th World conference on timber engineering (WCTE 2010). Riva del Garda (Italy), June 20–24; 2010. 10pp.
[5] Gurkšnys K. Development and testing of composite timber–concrete beams and connectors. Doctoral Dissertation, Vilnius; 2006, 95 p [in Lithuanian].
[6] Ceccotti A, Fragiacomo M, Giordano S. Behaviour of a timber–concrete composite beam with glued connection at strength limit state. In: Proceedings of the 9th world conference on timber engineering (WCTE 2006), Portland (USA), August 6–10; 2006. 8pp.
[7] Lukaszewska E, Fragiacomo M, Johnsson H. Laboratory tests and numerical analyses of prefabricated timber–concrete composite floors. J Struct Eng 2010;136(1):46–55.
[8] Negrão JHJO, MaiadeOliveira FM, LeitãodeOliveira CA, Cachim PB. Glued composite timber–concrete beams. ii: analysis and tests of beam specimens. J Struct Eng 2010;136(10):1246–54.
[9] Fragiacomo M, Amadio C, Macorini L. Short- and long-term performance of the "Tecnaria" stud connector for timber–concrete composite beams. Mater Struct 2007;40(10):1013–26.
[10] Fragiacomo M, Ceccotti A. Long-term behavior of timber–concrete composite beams. I: finite element modeling and validation. J Struct Eng 2006;132(13):13–22.
[11] Mueller J, Haedicke W, Simon A, Rautenstrauch K. Long-term performance of hybrid timber bridges – experimental and numerical investigations. In: Proceedings of the 10th world conference on timber engineering (WCTE 2008), Miyazaki (Japan), June 2–5; 2008. 8 pp.
[12] Jorge L, Cruz H, Lopes S. Tests in Timber-LWAC composite beams with screw-type fasteners. In: The 8th world conference on timber engineering (WCTE 2004), Lathi, Finland; 2004. 6pp.
[13] Rzhanicyn AR. Theory of build-up bars of building structures. Gostehizdat; 1948 [in Russian].
[14] Rzhanicyn AR. Build-up bars and plates. Stroiizdat: Moskow; 1986 [in Russian].
[15] EN 1995-1-1:2005: Eurocode 5: Design of timber structures – Part 1-1: General – Common rules and rules for buildings. Brussels: CEN; 2005.
[16] Kreuzinger H. Mechanically joined beams and columns. In: Blas, HJ, Aune P, Choo BS. et al., editors. Timber engineering – Step. Almere: Centrum Hout, 1995. p.B11/1- B11/8.
[17] Davids WG. Nonlinear analysis of FRP–glulam–concrete beams with partial composite action. J Struct Eng 2001;127(8):967–71.
[18] Kroflič A, Planinc I, Saje M, Turk G, Čas B. Non-linear analysis of two-layer timber beams considering interlayer slip and uplift. Eng Struct 2010;32(6):1617–30.
[19] Miller JF, Bulleit WM. Analysis of mechanically laminated timber beams using shear keys. J Struct Eng 2011;137(1):124–32.
[20] Chui YH, Barclay DW. Analysis of three-layers beams with non-identical layers and semi-rigid connections. Can J Civil Eng 1998;25:271–6.
[21] Taheri M, Barros JAO, Salehian H. A design model for strain-softening and strain-hardening fiber reinforced elements reinforced longitudinally with steel and FRP bars. Compos Part B: Eng 2011;42(6):1630–40.
[22] Balevičius R. Semi analytical modeling of reinforced concrete members in bending. Mechanika 2005;55(5):32–40.
[23] CEB-FIP Model Code 1990: Design Code. Thomas Telford Ltd.; 1993.
[24] Dias AMPG, Jorge LFC. The effect of ductile connectors on the behaviour of timber–concrete composite beams. Eng Struct 2011;33(11):3033–42.
[25] EN 1992-1-1:2004: E. Eurocode 2: Design of concrete structures – part 1–1: Gecneral rules and rules for buildings. Brussels: CEN; 2004.
[26] Dinwoodie J. Timber: nature and behaviour. Taylor & Francis; 2000.
[27] Thelandersson S, Larsen HJ. Timber engineering. Wiley; 2003.
[28] Clarke JL, editor. Structural design of polymer composites: eurocomp design code and background document. Taylor & Francis; 1996.
[29] EN 338:2009. Structural timber – strength classes. Brussels: CEN; 2009.
[30] ACI Committee 318. Building Code Requirements for Structural Concrete (ACI 318–05) and Commentary (ACI 318R-05). American Concrete Institute; 2005.